Journal of Applied Fluid Mechanics, Vol. 16, No. 11, pp. 2290-2299, 2023.
Available online at www.jafmonline.net, ISSN 1735-3572, EISSN 1735-3645.
https://doi.org/10.47176/jafm.16.11.1874

Numerical Simulation of Underwater Supersonic Jet of Vehicle with Shell-Shaped Flow Control Structure

C. Ruixiang[1], X. Muyao[2], W. Ying[1†], Y. Chao[2], Y. Bin[1] and L. Shipeng[3]

[1] *School of Energy and Power Engineering, University of Shanghai for Science and Technology, Shanghai 200093, China*
[2] *Shanghai Space Propulsion Technology Research Institute, Shanghai 201109, China*
[3] *School of Aerospace Engineering, Beijing Institute of Technology, Beijing 100081, China*

†*Corresponding Author Email: wangying@usst.edu.cn*

ABSTRACT

When the underwater vehicle engine operates under the condition of over-expansion, the violent pulsation of the flow field pressure at the rear of the nozzle can cause violent fluctuations in engine thrust, leading to engine instability. In order to improve the engine's stability, this study drew inspiration from the wave attenuation characteristics of the shell-shaped surface texture structure and added a multi-layer shell-shaped texture structure to the rear wall to reduce pressure fluctuations in the flow field at the rear of the nozzle . Based on the numerical simulation method, the effects of different bionic shell-shaped structures on jet morphology, wall pressure and engine thrust were compared and analyzed. The results show that the multi-layer bionic shell-shaped texture structure can effectively inhibit the occurrence of periodic phenomena such as bulge, necking, and return stroke in the rear flow field, so as to effectively reduce the pressure fluctuation in the rear flow field of the nozzle. In addition, when the momentum thrust is almost unchanged, it is found through calculations that during the initial stage of the jet, the suppression of thrust is not significant. After 0.005 seconds, the oscillation amplitude of the combined force of pressure difference thrust and back pressure thrust decreased by 22%, and the oscillation amplitude of the total thrust decreased by 20%.

Article History

Received March 26, 2023
Revised July 10, 2023
Accepted July 11, 2023
Available online September 3, 2023

Keywords:
Underwater vehicle engine
Shell-shaped medium
Pressure pulsation
Numerical simulation
Flow control

1. INTRODUCTION

The solid rocket motor represents a convenient and simple propulsion device for underwater vehicles. When operating underwater, the density of the external water environment is large, and the gas ejected from the nozzle will encounter great resistance in the jet process. Due to two-phase interface interaction, the tail flow field will undergo dramatic changes, which will cause the loss of thrust and affect the stability of underwater vehicles. Therefore, it is necessary to control and reduce the pressure pulsation of the underwater engine through certain flow control methods to improve its stability.

Global scholars have conducted experiments and numerical simulations of the underwater supersonic jet. According to Tang et al. (2012) , during the initial phase of engine ignition, high-temperature combustion bubbles appear at the nozzle tail. The expansion of these bubbles results in pressure reduction, leading to a pressure difference between the front and rear end faces that causes negative thrust. Wang et al. (2019) conducted numerical simulation research by selecting nozzle models with different expansion ratios. It was found that nozzle tail jet shapes varied among different expansion ratios, the low expansion ratio nozzle showed higher back pressure oscillation frequency and more stable thrust, contributing to more effective underwater propulsion. He et al. (2014) used the visualization method of high-speed video to study the development of the gas bubble at the outlet of the underwater gas jet and the dynamic instability of the jet. Tang et al. (2016) discovered that the peak value of engine thrust spectrum is related to the periodic change of underwater gas jet morphology through numerical simulation under different working conditions. Zhang et al. (2019) used the mixture multiphase flow model to conduct a two-dimensional axisymmetric numerical simulation of underwater supersonic flow. They found that the periodic oscillation of the flow field at the nozzle tail is due to the formation of a strong compression zone on the gas-liquid interface by gas-liquid impact, which is caused by the back propagation of the pressure wave of continuous impact. Shi et al. (2010) conducted an experimental study of the underwater supersonic gas jet, found that the supersonic gas jet injected into the water is

Nomenclature

A_e	outlet area	s	texture spacing
A_s	tail area	T	temperature
D	diameter of the nozzle outlet	u_i, u_j	velocity components
F	thrust	U	velocity
F_i	source term	v	kinematic viscosity of water
G	production term	Y	diffusion term
h	texture depth	s	texture spacing
k	turbulent kinetic energy	Z	cross diffusion term
$\dot{m}$	mass flow of outlet gas	α_g	gas phase volume fraction
p	pressure	α_w	liquid phase volume fraction
p_e	static outlet pressure	φ_m	physical property of the mixed phase
p_h	ambient pressure	ω	turbulent dissipation rate
S	user-defined source term	Γ	effective diffusion coefficient

always accompanied by strong flow oscillation, and proposed that this is related to the shock wave feedback phenomenon in the gas. Xu et al. (2020) established the numerical calculation model of floating mine under different working conditions, and found that the position of the gas jet necking and bulging phenomenon from the nozzle outlet various working conditions. That is, when the necking and bulging phenomenon was away from the nozzle outlet, the engine thrust oscillation was not violent; When the necking and bulge phenomenon is close to the nozzle outlet, the engine thrust oscillates violently. Zhang et al. (2021) used the VOF multiphase flow model to simulate the gas-water two-phase coupling, and found that in the process of the underwater gas jet ejection, the Kelvin Helmholtz (K-H) instability at the gas-water interface dominated by velocity gradient gradually changed into the Rayleigh Taylor (R-T) instability dominated by gravity and buoyancy. The research of the above scholars is focused on the change of flow field and jet structure at the tail of the underwater supersonic jet, and they all analyze the jet's structural characteristics at the nozzle's tail from the mechanism. However, the drastic change of the underwater engine's wake field will aggravate its performance's instability. So it is urgent to develop a flow control method to reduce the pressure pulsation of the flow field and improve the stability of the underwater nozzle.

Flow control methods are primarily categorized into passive control and active control. The passive control requires additional mechanical structure, while the active control entails energy input to regulate flow by controlling energy input. In terms of active control, Xu et al. (2021) proposed ventilated supercavitation to control the flow of the nozzle's flow, and found that the periodic change of the wake field was significantly reduced and the stability of the engine was improved. Li et al. (2021) used the phenomenological model to simulate the effect of plasma excitation to numerically study the inhibition effect of plasma exciter on the nozzle's separation flow. He found that the arc discharge plasma has a good effect on inhibiting the separation flow of the nozzle. Wang et al. (2010) conducted experiments and numerical simulations to study the impact of different nozzle profiles on separated flow. They found that conical nozzles are susceptible to flow separation, demonstrating that the nozzle flow pattern also affects nozzle flow separation. Boccaletto (2008) suppressed nozzle flow separation using annular plug airflow at the nozzle's end.

Regarding passive control, Wu and Huang (2022) used the ejector with simplified geometric model for flow control. They found that the nozzle could be in full flow working state after using the ejector. Zhou et al. (2015) employed the passive cavity structure in the single expansion inclined plane nozzle. They found that the existence of the passive cavity structure promoted the flow separation of the nozzle, reduced the number of shock waves in the single expansion inclined plane nozzle and improved the axial thrust coefficient of the nozzle. Sato et al. (2007) proposed using an extendable nozzle to achieve greater specific impulse and height compensation to curb flow separation. However, there is little research on underwater supersonic gas jet flow control. Because the jet gas in the underwater supersonic gas jet will interact with the water medium to form a complex gas-liquid interface, and the interaction between the two phases is more complex. So it is difficult to find a suitable flow control method to control the instability of its wake.

In nature, the shell-shaped surface texture structure is an effective mean of flow control. Its influence on flow is realized by non-smooth structure. Zhang et al. (2013) conducted numerical simulations to research different shell surface texture structures and found that the flow control effect of rectangular groove surface structure was the most effective. Li et al. (2002) found that the comb shell-shaped structure can reduce the wave reflection and the comb structure's stress through experimental research. Wan et al. (2022) established the numerical model of wave and comb structure based on OpenFOAM, revealing that the comb structure has excellent characteristics of wave dissipation and reducing wave reflection. The environment of the shell-shaped is the same as that of the underwater engine. Inspired by the wavy pattern on the

surface of the shell-shaped with better flow control effect, this structure is arranged on the rear wall of the nozzle to achieve the purpose of flow control and improve the stability of the nozzle wake.

In this paper, the shell-shaped surface texture structure is applied to the rear nozzle wall of the underwater vehicle to control the flow. The underwater vehicle model with the shell-shaped surface wavy texture flow control structure is established. The changes of nozzle wall pressure, rear flow field, velocity field and thrust are studied by numerical simulation. The research results can provide a reference for the development of the next generation of underwater vehicle engine with high stability.

2. CALCULATION MODEL

2.1 Control Equations

In the underwater supersonic gas jet, the gas is set as the ideal gas model calculation, and the liquid phase is set as water. Both buoyancy and surface tension are considered. Continuity equation, momentum conservation equation, energy conservation equation and volume transport equation are as follows:

$$\frac{\partial \rho_m}{\partial t}+\frac{\partial(\rho_m u_i)}{\partial x}=0 \tag{1}$$

$$\frac{\partial(\rho_m u_i)}{\partial t}+\frac{\partial(\rho_m u_i u_j)}{\partial x}=-\frac{\partial p}{\partial x_i}+\frac{\partial}{\partial x_i}\left[\mu_m\left(\frac{\partial u_i}{\partial x_j}+\frac{\partial u_j}{\partial x_i}\right)\right]+S_i \tag{2}$$

$$\frac{\partial}{\partial t}\sum_{n=w,g}(\alpha_n\rho_n E_n)+\frac{\partial}{\partial x_j}u_j\sum_{n=w,g}[\alpha_n(\rho_n E_n+p)]=\frac{\partial}{\partial x_j}\left(k_{eff}\frac{\partial T}{\partial x_j}\right) \tag{3}$$

$$\frac{\partial}{\partial x_j}(\alpha_g\rho_g)+\frac{\partial}{\partial x_i}(\alpha_g\rho_g u_i)=0 \tag{4}$$

where p is the pressure, T is the temperature, u_i and u_j are the velocity components, F_i is the source term, φ_m is the physical property of the mixed phase, and $\varphi_m=\varphi_g\alpha_g+\varphi_w(1-\alpha_g)$; φ_g and φ_w are the gas phase density or viscosity coefficients, as well as liquid phase density or viscosity coefficient; α_g and α_w are the gas phase volume fraction and liquid phase volume fraction, and $\alpha_g+\alpha_w=1$.

2.2 Turbulence Model

This paper uses the k-ω SST turbulence model to close the Reynolds averaged N-S equation. This turbulence model is based on the standard *k*- *ω* and *k*- *ε*, which are combined to activate *k*-*ω* mode when simulating near wall region and use the k- ε model when solving in the far field. The model equation is as follows:

$$\frac{\partial}{\partial t}(\rho k)+\frac{\partial}{\partial x_i}(\rho k u_i)=\frac{\partial}{\partial x_i}(\Gamma_k\frac{\partial k}{\partial x_i})+G_k-Y_k+S_k \tag{5}$$

$$\frac{\partial}{\partial t}(\rho\omega)+\frac{\partial}{\partial x_i}(\Gamma_w\frac{\partial \omega}{\partial x_i})+G_w-Y_w+Z_w+S_w \tag{6}$$

where k is the turbulent kinetic energy, ω is the turbulent dissipation rate, Γ is the effective diffusion coefficient, G is the production term, Y is the diffusion term, Z is the cross diffusion term, and S is the user-defined source term.

2.3 VOF Model

VOF model simulates two or more immiscible fluids through momentum and phase volume fraction equations. Fluids share a set of momentum equations. In the calculation process, the phase volume fraction is introduced to track the phase interface of each calculation unit. For phase q, the volume ratio equation is:

$$\frac{1}{\rho_q}\left[\frac{\partial}{\partial t}(\alpha_q\rho_q)+\nabla(\alpha_q\rho_q v_q)\right]=S_{\alpha_q}+\sum_{p=1}^{n}(\dot{m}_{pq}-\dot{m}_{qp}) \tag{7}$$

where $\dot{m}_{pq}$ represents the mass transfer from the q^{th} phase to the p^{th} phase, and $\dot{m}_{qp}$ represents the mass transfer from the p^{th} phase to the q^{th} phase. Generally, the source term at the right end of the equation is zero. The main phase volume ratio is subject to the following constraints:

$$\sum_{q=1}^{n}\alpha_q=1 \tag{8}$$

In this paper, the gas phase is an ideal compressible gas with a dynamic viscosity of 1.784×10^{-5}pa·s, the liquid phase is water, the density is 998.2kg/m^3, and the dynamic viscosity is 1.003×10^{-3}pa·s.

2.4 Geometry Model and Calculation Conditions

2.4.1 Geometry Model

The research shows that the main mechanism of wave dissipation by textured groove is the influence of non-smooth structures on flow. Walsh (1983) of NASA Langley center measured some parameters through experiments: when the dimensionless dimension $h^+>25$ and $s^+>30$ of the depth h and spacing s of the shell-shaped texture structure have the effect of increasing the resistance.

h^+, s^+ is defined as:

$$h^+=0.172\frac{h\cdot U\cdot {Re_x}^{-0.1}}{v} \tag{9}$$

$$s^+=0.172\frac{s\cdot U\cdot {Re_x}^{-0.1}}{v} \tag{10}$$

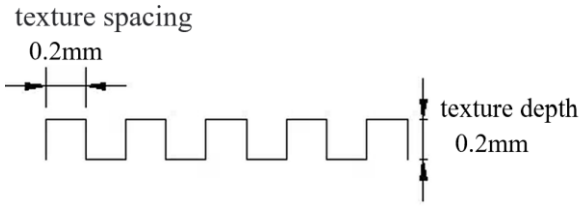

Fig. 1 Bionic dimension diagram of shell-shaped surface

Fig. 2 Original shell-shaped

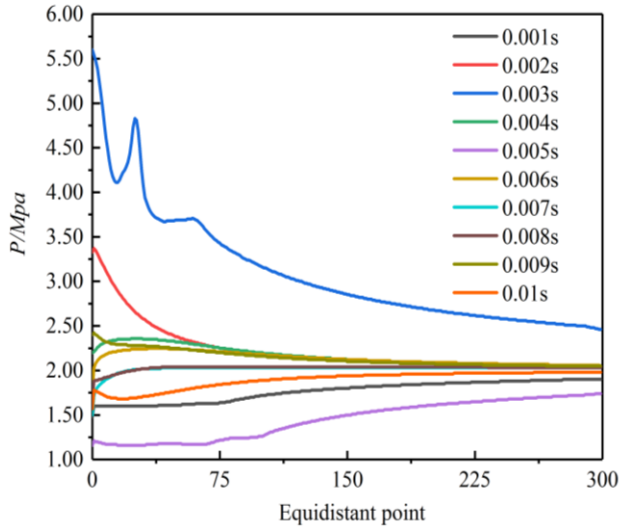

Fig. 3 Pressure at different positions of lower wall at different times

The dimensions of the shell-shaped groove are shown in Fig.1. The texture depth of the rectangular groove is h=0.2mm, and the texture spacing is s=0.2mm. Because the wake of an underwater engine is a typical hypersonic gas jet, and the Reynolds number at the gas phase outlet is as high as 10^8(Zhang et al., 2020). The Reynolds number is $Re=10^8$ and kinematic viscosity of water $v=1\times10^{-6}$N·s/m^2; At the same time, according to the numerical simulation results, the incoming flow velocity U=40m/s. Therefore, according to equations (9)-(10), the dimensionless dimensions h^+=218>25 and s^+=218>30 can be obtained. From the perspective of dimensionless dimensions, these designed dimensions result in an increased resistance effect.

For the actual shell shape, as shown in Fig. 2, the surface texture is not the same. In this paper, 300 equidistant points are taken from the nozzle wall to simultaneously analyze the pressure at different points. In Fig. 3 it is found that the pressure changes greatly from the nozzle outlet to one-third of the wall, so a multi-layer shell-shaped texture structure is arranged at this position. The specific shell-shaped groove size and layout position are shown in Fig. 4. The texture height is designed as a staggered structure of 0.2mm and 0.4mm.In order to enhance the structural strength of the shell-shaped structure in subsequent practical applications, the texture height near the nozzle outlet is increased to 0.6mm.Due to the uncertainty of jet return stroke direction, the shell-shaped structure is placed in different directions increase its applicability. The geometric structure of the above design is stable and can be used for wave elimination better. At the same time, to ensure that different layers are not crowded, the distance between layers is half the length of the imitation shell-shaped, and the shell-shaped structure is located 2mm from the nozzle wall.

2.4.2 Calculation domain and boundary conditions

This paper uses the two-dimensional axisymmetric model for numerical simulation. The calculation domain is shown in Fig.5. The length of the whole computational domain is 400 times the nozzle outlet diameter, and the width is 200 times the nozzle outlet diameter. The nozzle inlet is subjected to the pressure boundary condition of 6.7Mpa, while the outlet is set to the pressure boundary condition of 2MPa, and the rest is the non-slip solid wall boundary condition. The calculation domain is initialized with water environment pressure. The whole computing area is divided into structured grids, as shown in Fig.6.

2.4.3 Calculation method

This paper adopts the finite volume method to discretize the governing equation. The separate solver and the simple algorithm of pressure-coupled equations are used to solve the control equation, and the body force weight algorithm is used to solve the control equation. The volume fraction equation uses the geo construct scheme, and the energy, momentum, and momentum equations use the second-order upwind discrete scheme.

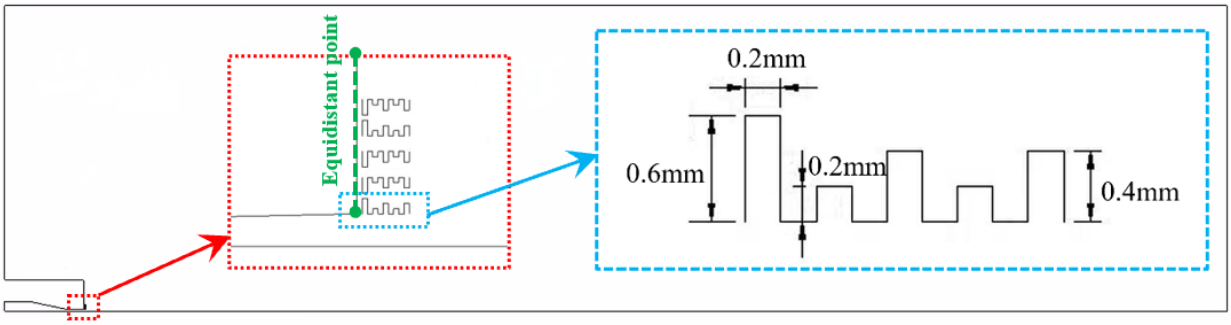

Fig. 4 Flow control structure size

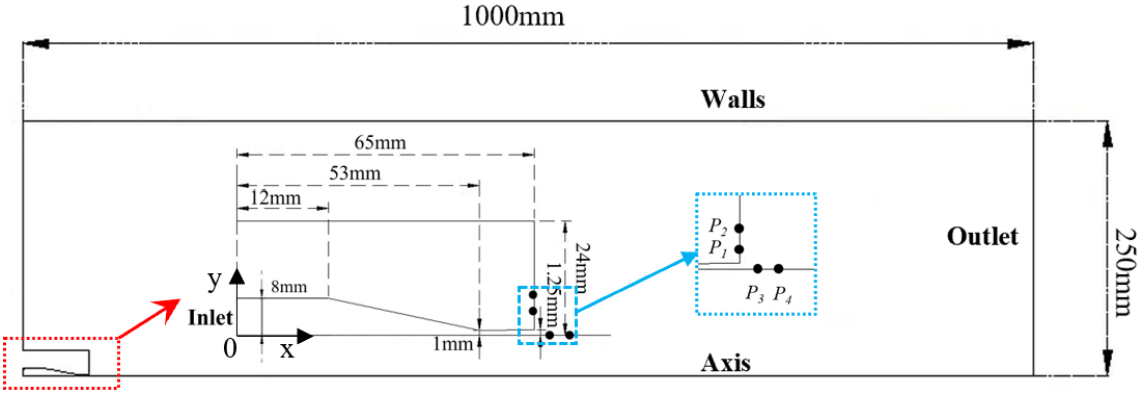

Fig. 5 Calculation domain and boundary conditions

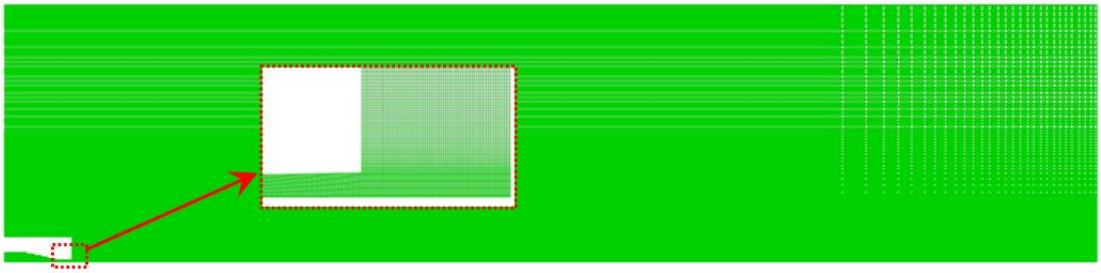

Fig. 6 Grid distribution

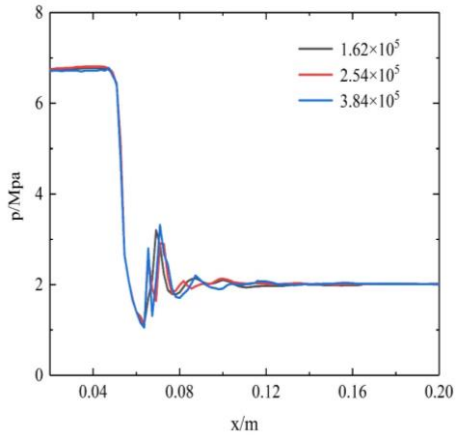

Fig. 7Axis pressure variation

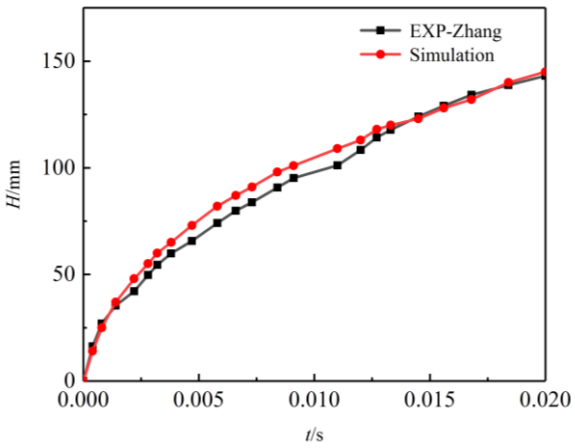

Fig. 8 Experimental and numerical simulation results of underwater jet height

2.5 Numerical Model Validation

Simulations using different grid sizes are conducted to evaluate grid independence. The pressure distribution on the streamline for each different grid size is shown in Fig. 7. The maximum error between 1.62×10^5 and 2.54×10^5 grids was within 3%, and the maximum error between 2.54×10^5 and 3.84×10^5 grids was less than 5%. Therefore, the grid pre-calculation results of the grid can be deemed as independent. To reduce computation costs, the grid size of 2.54×10^5 is chosen for further calculations.

In order to validate the accuracy of the numerical simulation results presented in this paper, the same experimental conditions for underwater jets as those reported by (Zhang et al., 2020) are adopted for verification. The experimental results of the underwater jet height measured under the experimental conditions in the literature are compared with the numerical simulation of the underwater jet height in this paper, as shown in Fig. 8. As evidenced by the figure, the results from the experiment and the numerical simulation tend to be in agreement, with a maximum error of less than 10%. Thus, it can be concluded that the numerical model proposed in this paper produces a superior prediction of the shape changes of the underwater jet.

2.6 Thrust Force Calculation Method

The method of calculating the thrust of an underwater vehicle is similar to that in air media. The thrust of the underwater vehicle is shown in Fig. 9 (Zhang et al., 2020). The engine of said underwater vessel will experience disparate levels of pressure on its front and rear surfaces. This variance in pressure will create a supplementary differential pressure thrust, so the thrust F of the underwater vehicle will be composed of gas thrust

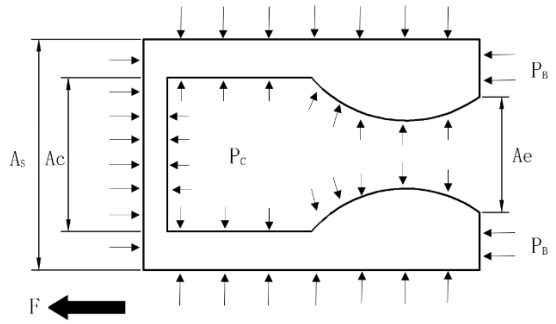

Fig. 9 Stress analysis diagram of underwater nozzle (Zhang et al. 2020)

F_1 generated by gases and differential pressure thrust F_2 generated by pressure difference.

$$F_1 = \dot{m}v_e \tag{9}$$

$$F_2 = (p_B - p_h)(A_s - A_e) + (p_e - p_h)A_e \tag{10}$$

$$F = \dot{m}v_e + (p_e - p_h)A_e + (p_B - p_h)(A_s - A_e) \tag{11}$$

where, $\dot{m}$ represents the mass flow of outlet gas, v_e represents the outlet speed, p_e represents the static outlet pressure, A_e represents the outlet area, p_h represents the ambient pressure, and A_s represents the tail area.

3. CALCULATION RESULTS AND ANALYSIS

The central point of focus for this paper lies in the stability of an underwater vehicle. In accordance with Wang et al. (2019) , the interaction between the water environment and the jet gas may induce pressure and thrust oscillation, thus posing a severe challenge to the vehicle's stability. Therefore, this paper aims to examine the stability of underwater vehicles from the variation characteristics of nozzle wall back pressure and thrust.

3.1 Pressure Analysis of Tail Flow Field

Firstly, an analysis of the influence of the shell-shaped structure on wall pressure fluctuation is conducted. In order to acquire pressure fluctuations within the downstream pressure field, various monitoring points are established on both the wall and axis, as displayed in Fig.5. The distance between two points P_1-P_2 on the wall and the nozzle outlet is *D* and 2*D,* correspondingly, where *D* is the diameter of the nozzle outlet. Two points P_3-P_4 are designated on the axis, with distance of *D* and 2*D,* respectively, from the nozzle outlet.

Figures 10 and Fig.11 compare the pressure values of the monitoring points on the tail wall and the axis before and after adding on imitation shell-shaped structure. For the nozzle without imitative shell-shaped structure, pressure oscillation near the nozzle outlet is more intense in both the axial and wall direction. However, the shell-shaped structure can suppress pressure fluctuation on both the wall and axis. From Fig. 10, the initial pressure oscillation on the wall is relatively violent. When the tail flow field further develops, the pressure on the wall gradually tends to 2MPa.

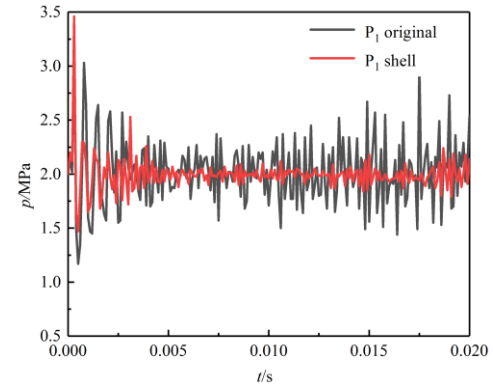

(a)P_1

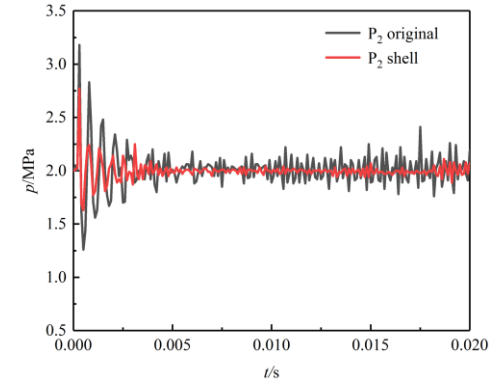

(b)P_2

Fig. 10 Comparison of pressure values at wall pressure monitoring points and non imitation shell-shaped structure.

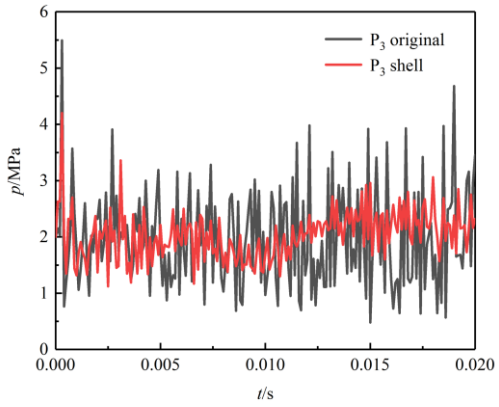

(a)P_3

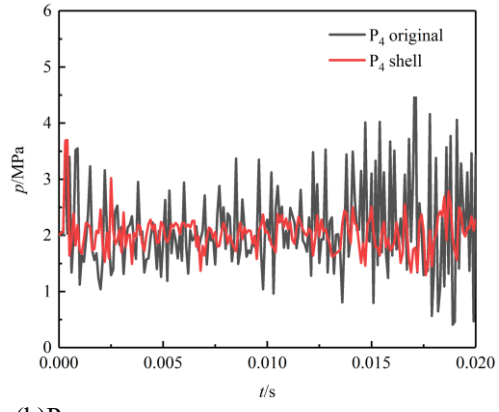

(b)P_4

Fig. 11 Comparison of pressure values at monitoring points along the axis with non imitation shell-shaped structure

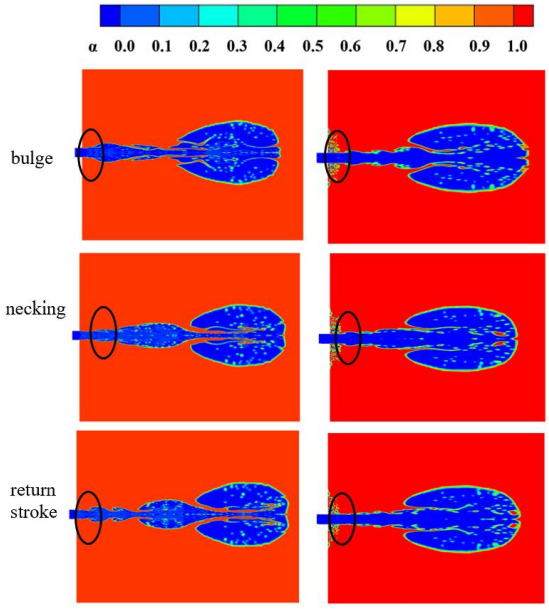

Fig. 12 Comparison of different stages of typical process of underwater gas jet

It can be seen from Fig. 11 that the closer to the nozzle outlet, the more intense the pressure oscillation and the greater the amplitude of the oscillation. However, after adding the shell-shaped structure, the amplitude of pressure oscillation decreased significantly. We used the oscillation amplitude as a measure of the strength of pressure pulsation, defined as the difference between the maximum and minimum pressure values after 0.005 seconds. For Fig. 10, at monitoring point P_1, the oscillation amplitude of pressure decreased by 43.5%, and at monitoring point P_2, the oscillation amplitude of pressure decreased by 55.3%. For Figure 11, at monitoring point P_3, the pressure oscillation amplitude decreased by 46.5%, and at monitoring point P_4, the pressure oscillation amplitude decreased by 46%。Therefore, we can further analyze the mechanism of the pressure fluctuation suppression of the nozzle wake by the shell-shaped structure from the typical phenomenon of the underwater jet morphology.

Figure 12 displays the typical evolution process of the underwater jet morphology. The evolution process of underwater jet morphology mainly consists of three stages: bulge, necking and return stroke. At the initial stage of the underwater jet's emergence the water environment obstructs the gas flow, thereby causing a high-pressure area to form at the nozzle outlet. This phenomenon forces the gas to flow backward and expand into an airbag. Following the occurrence of the bulge, the pressure of the gas within the airbag decreases, leading to differences pressure between the inside and outside, resulting necking. After necking, the path for the gas to flow becomes narrower, making gas movement more difficult. Thus, the gas pressure in the bubble increases, and the gas movement is blocked, resulting in a return stroke.

Regarding Fig.12, when the shell-shaped structure is added, the bulge phenomenon is restrained to a certain extent at the nozzle outlet. However, since necking occurs at a certain distance from the nozzle outlet, the shell-shaped structure has little effect on the necking phenomenon. When the underwater jet bubble breaks, part of the air flow will continue moving forward, while some will generate backflow and cause a return stroke. After the adding of the shell-shaped structure, the return stroke phenomenon is also restrained to a certain extent.

3.2 Analysis of Tail Flow Field

To analyze the influence of the shell-shaped structure on the flow field at the tail of the underwater jet, this paper examines changes in the tail outlet pressure under the three typical phenomena of the underwater jet flow field: bulge, necking and return stroke. Fig.13 depicts the contour when the gas volume fraction is 0.9.

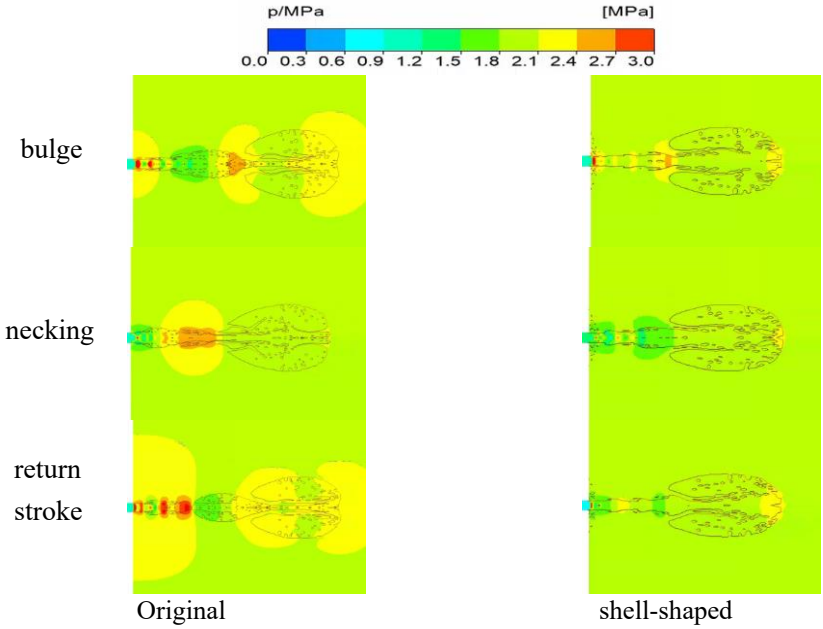

Fig. 13 Comparison of pressure nephogram of underwater gas jet

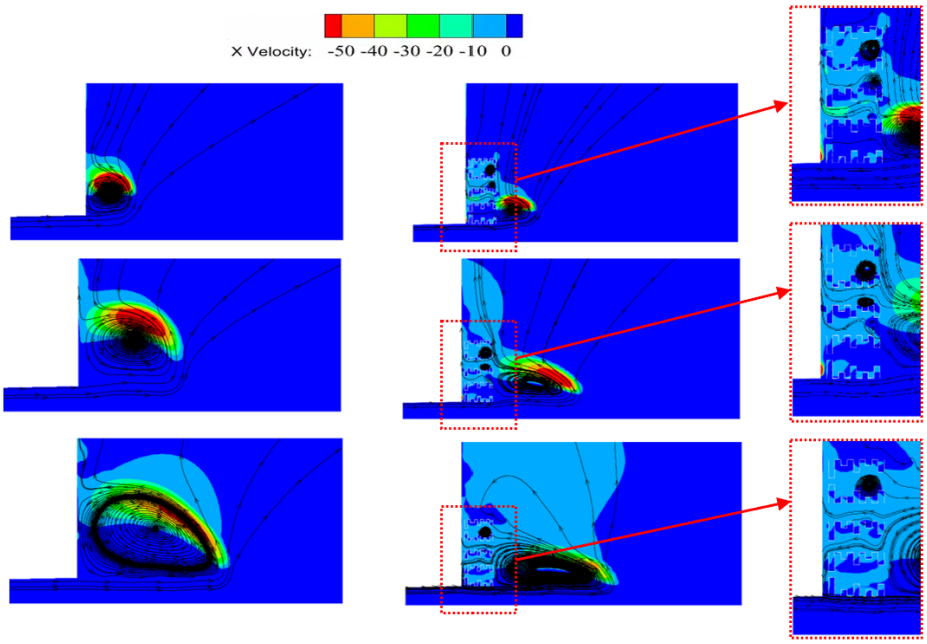

Original shell-shaped

Fig. 14 Local speed at tail part

At the initial stage of the jet formation, due to the weak ability of the gas to push through the water medium, a high-pressure area will generate near the wall at the nozzle outlet, and then an air bag will be formed, causing the gas to return. Upon adding the shell-shaped structure, the pressure on the outlet wall decreases. This occurrence is due to the fact that the gas in the initial airbag forms after passing through the shell-shaped structure. As the structure generates flow resistance, lesser amount of gas and liquid reach the nozzle wall, leading to a small high-pressure area at the nozzle wall.

The necking stage occurs far away from the nozzle outlet and has little effect on the pressure field on the nozzle wall. Hence, the presence or absence of shell-shaped structure has minimal influence on it. In the return stroke stage, due to the constriction of the gas channel after necking, some gas continues to move forward, while other gas returns to the wall, resulting in the formation of a large area of high pressure at the outlet wall of the nozzle. As a result of the shell-shaped structure, the outlet wall pressure is lower than that of the traditional nozzle.

From the above analysis, it can be inferred that the cyclical variations of the bulge, necking and return stroke phenomena at the rear of the nozzle cause pressure fluctuation on the nozzle wall. In addition, the shell-shaped structure has a restraining effect on the rear pressure fluctuation.

To further analyze the pressure fluctuation reduction mechanism fueled by the shell-shaped structure, we can refer to Fig.14 that after the gas pushes away the water medium at the nozzle outlet, the water becomes compressed towards the nozzle wall. This phenomenon lead to dramatic fluctuations in the wall pressure for both the structured and unstructured models. This phenomenon will occur in both the unstructured and the shell-shaped structure models. It can be observed that the unstructured model's

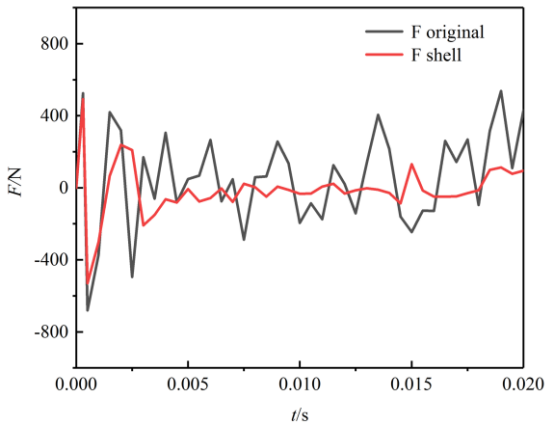

Fig. 15 Total thrust comparison

wall has a greater reverse velocity in the x-axis direction. As the inverse velocity in the x-axis direction of the shell-shaped structure model approaches the wall, it starts to decrease towards zero. As a result, the pressure fluctuation on the nozzle wall gradually approaches the environmental value, thereby reducing the wall's pressure fluctuation.

3.3 Thrust Analysis

Figure15 depicts the thrust curve of the underwater vehicle with time. Due to the instantaneous ejection of the gas jet, the initial stage results in a peak thrust. After reaching the maximum, the thrust began to violently fluctuate. The primary reason for the violent oscillation is the flow field behind the nozzle has bulged, necked and rebounded, resulting in the sharp change of the nozzle outlet pressure. This will affect the violent oscillation of nozzle thrust. As shown in Fig. 16, after incorporating the shell-shaped structure, although oscillations persist, the thrust exhibits some reduction in fluctuation during the stable phase after the peak thrust appears. Based on the

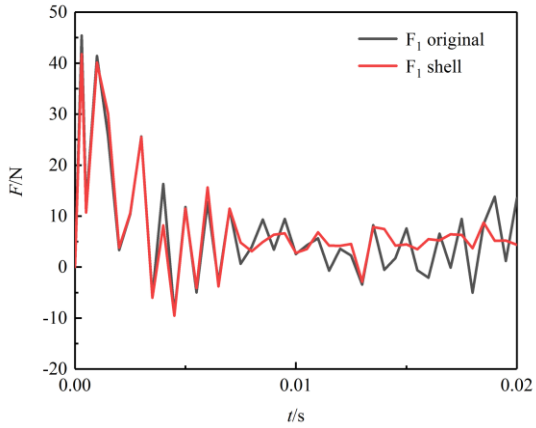

Fig. 16 Momentum and thrust comparison

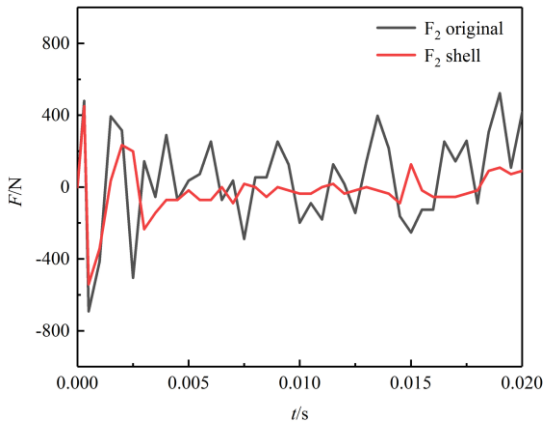

Fig. 17 Comparison of differential pressure and back pressure thrust

thrust calculation method stated above, it generates three parts. Firstly, the first part is the thrust generated by gas, which is called momentum thrust F_1. The second part of the thrust generated by differential pressure is called differential pressure thrust, and the last part generated by back pressure is called back pressure thrust. The sum of differential pressure thrust and back pressure thrust is F_2, as shown in Fig.17. As demonstrated, the shell-shaped structure does not influence momentum thrust but has a prominent effect on differential pressure thrust and back pressure thrust. Due to the existence of the shell-shaped structure, the pressure pulsation generated on the nozzle tail wall is weakened, which reduces the amplitude of the engine-generated back pressure oscillation. Research proves that the shell-shaped structure mitigates underwater vehicle thrust oscillation and enhances stability.

4. CONCLUSION

The present paper draws inspiration from wave structures' flow control on the shell-shaped surface and applies them to enhance underwater vehicle stability via nozzle rear wall modifications. Specifically, the paper sets up a multi-layer shell-shaped corrugated structure on the rear wall of the nozzle. By analyzing the pressure field and velocity field, the mechanism by which the shell-shaped structure reduces the thrust oscillation of the engine nozzle and improves the stability of the underwater vehicle is explored, and the following conclusions are drawn.

(1) When no shell-shaped structure is present, an over-expanded state causes periodic phenomena, --such as bulge, necking, and return stroke--, to occur in the flow field behind the nozzle. By adding the shell-shaped structure to the nozzle tail, the bulge and return stroke phenomena occurrences are reduced.

(2) The study concludes that the shell-shaped structure can restrain the pressure fluctuation on the nozzle wall, thereby ensuring the engine thrust does not oscillate violently, improving overall engine stability.

(3) The impact of the two-phase flow at the nozzle tail on the nozzle wall can be reduced by installing the shell-shaped structure to synchronously reduce the engine thrust oscillation and the wake field oscillation. After 0.005 seconds, the oscillation amplitude of the combined force of pressure difference thrust and back pressure thrust decreased by 22%, while the oscillation amplitude of the total thrust decreased by 20%.

ACKNOWLEDGEMENTS

This study was supported by the Natural Science Foundation of Shanghai (Grant No. 20ZR1455200).

CONFLICT OF INTEREST

The authors have no conflicts to disclose.

AUTHORS CONTRIBUTION

Chu Ruixiang: Investigation, Writing – Original Draft; Xue Muyao: Investigation, Resources; Wang Ying: Supervision, Writing - Review & Editing; Yin Chao: Investigation, Resources; Yang Bin: Resources, Project administration; Li Shipeng: Resources

REFERENCES

Boccaletto, L. (2008). *Solving the flow separation issue: a new nozzle concept*. 44th AIAA/ASME/SAE/ASEE Joint Propulsion Conference & Exhibit , 5234. https://doi.org/10.2514/6.2008-5234

He, M., L. Qin, J., He., X. Zhang & Y. Liu (2014). Instablity of a transient submerged jet in supersonic nozzle during its start-up and shut-down process. *Journal of Propulsion Technology*, 523-529.

Li, C., F. Li., B. Yang & Y. Wang (2021). Numerical investigation of nozzle flow separation control using plasma actuation. *Acta Aeronautica et Astronautica Sinica*, 42(07), 228-238. https://doi.org/10.7527/S1000-6893.2020.24547

Li, Y., Z. Sun., S. Xu., G. Dong., Y. Lin., E. Niu & K. Mao (2002). The hydraulic performance of comb-type vertical breakwater. *Journal of Hydrodynamics*, (04), 472-482

Sato, M., Moriya, S. I., Tadano, M., Sato, M., Masuoka, T., & Yoshida, M. (2007). *Experimental study on transitional phenomena of extendible nozzle*. 43rd AIAA/ASME/SAE/ASEE Joint Propulsion Conference & Exhibit, 5471. https://doi.org/10.2514/6.2007-5471

Shi, H., B. Wang & Z. Dai (2010). Research on the mechanics of underwater supersonic gas jets. Science China Physics. *Mechanics and Astronomy*, 53, 527-535. https://doi.org/10.1007/s11433-010-0150-x

Tang, J., S. Li & N. Wang (2012). Study on the negative thrust of the underwater solid rocket engines. *Journal of Solid Rocket Technology*, 35(03), 325-329+343.

Tang, Y., S. Li, Z. Liu, X. Sui & N. Wang (2016). Research on thrust fluctuation characteristics of underwater solid rocket motor. *Journal of Solid Rocket Technology*, 39(04), 476-481. https://doi.org/10.13224/j.cnki.jasp.2017.02.028

Walsh, M. J. (1983). Riblets as a viscous drag reduction technique. *AIAA Journal*, 21(4), 485-486. https://doi.org/10.2514/3.60126

Wan, X., X. Li, T. Xie, J. Sun, X. Xie & Z. Cheng (2022). Hydrodynamic characteristics comparison of caisson-type and comb-type breakwater based on OpenFOAM. *Port & Waterway Engineering*, (06), 1-8. https://doi.org/10.16233/j.cnki.issn1002-4972.20220530.035

Wang, L., Y. Liu, D. Li, Q. Wu & G. Wang (2019). Numerical study of underwater supersonic gas jets for solid rocket engine. *Acta Armamentarii*, 40(06), 1161-1170. https://doi.org/10.2514/6.2021-1441

Wang, Y., F. Bao & J. Du (2010). Numerical simulation and experiment of flow separation in SRM nozzle. *Journal of Solid Rocket Technology*, 33(04), 406-408.

Wu, C., & X. Huang (2022). Numerical study of nozzle flow with large expansion ratio based on passive injection. *Aeronautical Science & Technology*, 33(10), 31-37. https://doi.org/10.19452/j.issn1007-5453.2022.10.004

Xu, H., K. Luo, C. Huang, Z. Zuo and X. Dong (2021). Influence of ventilated supercavitation on underwater rocket engine. *Journal of Harbin Institute of Technology*, 53(06), 41-47.

Xu, H., K. Luo, F. Liu, Z. Zuo, J. Gu & C. Huang (2020). Effects of underwater supersonic jet on force characteristics of floating mine. *Journal of Propulsion Technology*, 41(11), 2623-2629. https://doi.org/10.13675/j.cnki.tjjs.200397

Zhang, H., Z. Guo, R. Wang & Z. Chen (2019). Initial flow characteristics of an underwater supersonic gas jet. *Journal of Vibration and Shock*, 38(06), 88-93+131. https://doi.org/10.13465/j.cnki.jvs.2019.06.013

Zhang, X., S. Li., B. Yang & N. Wang (2020). Flow structures of over-expanded supersonic gaseous jets for deep-water propulsion. *Ocean Engineering*, 213, 107611. https://doi.org/10.1016/j.oceaneng.2020.107611

Zhang, X., S. Li, B. Yang, N. Wang, Q. Zheng, Y. Wang & Y. Tong (2021). Flow structures of vertical gaseous jets and effects of thrust of underwater solid rocket motor. *Journal of Propulsion Technology*, 42(05), 961-969. https://doi.org/10.13675/j.cnki.tjjs.190639

Zhang, X., X. Bai, C. Yuan & X. Yan (2013). Simulation analysis on drag reduction effect of shell surface texture with function of anti-fouling. *Shipbuilding of China*, 54(04), 146-154.

Zhou, L., H. Xiao, Z. Wang & Z. Liu (2015). Effects of passive cavity on high pressure ratio single expansion ramp nozzle. *Journal of Aerospace Power*, 30(08),1811-1817. https://doi.org/10.13224/j.cnki.jasp.2015.08.003